ISH Journal of Hydraulic Engineering

ISSN: 0971-5010 (Print) 2164-3040 (Online) Journal homepage: www.tandfonline.com/journals/tish20

Experimental hydraulic study for the effect of radial gates operation scheme on flow characteristics

Ahmed M. Ibraheem & Mohamed M. Ibrahim

To cite this article: Ahmed M. Ibraheem & Mohamed M. Ibrahim (25 Nov 2025): Experimental hydraulic study for the effect of radial gates operation scheme on flow characteristics, ISH Journal of Hydraulic Engineering, DOI: 10.1080/09715010.2025.2591665

To link to this article: https://doi.org/10.1080/09715010.2025.2591665

Published online: 25 Nov 2025.

ISH JOURNAL OF HYDRAULIC ENGINEERING
https://doi.org/10.1080/09715010.2025.2591665

Taylor & Francis
Taylor & Francis Group

Experimental hydraulic study for the effect of radial gates operation scheme on flow characteristics

Ahmed M. Ibraheem [a] and Mohamed M. Ibrahim [b]

[a]National Water Research Center, Hydraulics Research Institute, Shoubra El-Kheima, Egypt; [b]Shoubra Faculty of Engineering, Benha University, Shoubra, Egypt

ABSTRACT

The Egyptian irrigation system considers barrage regulators important structures for controlling flow discharge and upstream/downstream water levels. This study presents an experimental model simulating flow across radial gates, focusing on how symmetric and asymmetric gate operation schemes influence hydraulic behavior. A total of 80 test runs were performed using five gate-operating schemes under 16 flow conditions, including four tailwater depths (0.21, 0.23, 0.25, and 0.27 m) and four discharges (26, 29, 32, and 35 L/s), while maintaining a constant upstream depth of 0.40 m. Results showed good agreement between measured and calculated discharge coefficients compared with previous studies. Gate operation symmetry, under similar expansion ratios, had minimal effect on the discharge coefficient. The contraction coefficient was inversely related to the gate leaf angle. The length of the hydraulic jump increased with the increase in the Froude number. The outcomes gave good agreement compared to other formulas under similar hydraulic conditions. The submergence ratio increased with the increase in the submerged hydraulic jump length. A regression analysis model was applied, and simple empirical equations were derived to predict the discharge coefficient and the hydraulic jump length under limited flow conditions.

ARTICLE HISTORY
Received 10 May 2025
Accepted 14 November 2025

KEYWORDS
Barrages; flume; radial gates; submerged flow characteristics; discharge coefficient

1. Introduction

Due to the lifetime of the main barrages on the River Nile, the increased demand on electricity production and the increased water demand and the resulted higher water head between the upstream and the downstream, the Ministry of Water Resources and Irrigation (MWRI) in Egypt decided to replace the old barrages by new ones equipped with radial gates due to their applicability (e.g., New Esna Barrage; New Naga Hammadi Barrage; New Assiut Barrage; New Dairut group Regulator; New Mowes Regulator).

Radial gates have multiple on the water control structures in the irrigation system, where they are used to control water levels and flow discharges. Radial gates have many benefits compared to traditional sluice gates because they need a small hoisting force, easy operation, low disturbance, and higher conveyed discharge (Sehgal 1996; Babaei et al. 2021). The flow through the radial gates is categorized as free flow or submerged flow based on the gate opening and tailwater depth. Many studies have been done to explore the hydraulics of radial gates (e.g., Buyalski 1983; Clemmens et al. 2003; Bijankhan et al. 2011; Clemmens and Wahl 2012; Bijankhan et al. 2013; Ali et al. 2015).

Many publications have considered the flow characteristics of submerged hydraulic jumps (e.g., Narasimhan and Bhargara 1976; McCorquodale and Khalifa 1980; Ma et al. 2001; Abdel-Aal 2004; Bhuiyan et al. 2011; Abdelhaleem 2016).

Toch (1955) derived an empirical equation related the contraction coefficient, C_c, to the leaf angle, θ of sharp radial gates operating under free-flow conditions. The contraction coefficient in open-channel flow is a dimensionless number that quantifies the reduction in flow area and the resulting velocity increase when water flows from a wider section to a narrower section across the channel. The contraction coefficient indicates how much the flow contracts as it passes through a restriction.

CONTACT Ahmed M. Ibraheem eng.ahmedmahmoud2009@yahoo.com

$$C_c = 1 - 0.75\left(\frac{\theta^\circ}{90}\right) + 0.36\left(\frac{\theta^\circ}{90}\right)^2 \quad (1)$$

Where C_c is the contraction coefficient

Rajaratnam and Subramanya (1967) experimentally tested the single gate under free and submerged flow conditions. Equations (2) and (3) have been developed for calculating the discharge coefficient, C_d, and expansion ratio, e.

$$C_d = \frac{Q}{W * b_t\sqrt{2g * H}} \quad (2)$$

Where: Q; is the flow discharge, b_t; is the total clear width of opened gates, w; is the gate opening, H; is the head difference between upstream water depth and tailwater depth,

For more details, the total clear width, b_t, it equals the distance between piers from inside to inside multiplied by the number of opening gates. Noting that, the number of opening gates is varied according to the tested flow regime.

$$e = \frac{\text{TotalWidth}}{\text{No} \cdot \text{ofopenedgates} * \text{gatewidth}} \quad (3)$$

Where: e; is the expansion ratio

Bos (1989) and Lin et al. (2002) defined the distinguishing condition as the maximum tailwater level that allows the free flow downstream of a gate before the flow becomes submerged. They derived a generic formula based on the hydraulic jump concept to distinguish the flow condition of a radial single and multi-gates, as shown in Eq. (4):

$$\frac{y_t}{w} = \frac{\delta}{2}\left[\sqrt{1 + 16\left(\frac{H_u}{\delta\ w} - 1\right)} - 1\right] \quad (4)$$

Where: y_t; is the tailwater depth, δ; is the contraction coefficient, H_u; is the upstream water depth, and w; is the gate opening height.

Rajaratnam and Subramanya (1967) and Swamee (1992) derived the distinguishing conditions of a sluice gate for constant contraction coefficients of 0.61 and 0.6, respectively.

Tel (2000) developed Eq. (5) for calculating the contraction coefficient of sharp radial gates under free-flow conditions

$$\delta_{sh} = 1.001 - 0.2349\theta_r - 0.1843\theta_r^2 + 0.1133\theta_r^3 \quad (5)$$

Where: δ_{sh} is the contraction coefficient
θ_r is the gate leaf angle (in radian)

$$\theta_r = \text{ACOS}\left(\frac{(\text{Gate Axis Level} - \text{Sill gate level}) - \text{Gate opening}}{\text{Radius of Gate}}\right) \quad (6)$$

The influence of stilling basin geometry on the submerged hydraulic jump length, energy dissipation, and flow velocity was studied experimentally by (Ali et al. 2008; Ali and Mohamed 2010). The findings revealed that the flat apron is superior to the apron with a sill under the gate, focusing on the energy dissipation.

The distinguishing condition curve of radial gates was presented by Bijankhan et al. (2011). The distinguishing condition curve determines the conveyed flow type by involving the Energy and Momentum (E-M) principle. Habibzadeh et al. (2011) developed an equation to determine the discharge coefficient for sluice gates in rectangular channels under orifice flow utilizing a theoretical approach and (E-M) equations. The driven equation was applicable for free and submerged flow conditions.

Bijankhan et al. (2013) derived an equation to calculate C_d for submerged flow through radial gates without sill with coefficient of determination, $R^2 = 0.92$ and the mean absolute error = 1.89%.

$$C_d = \frac{\left[a_1 \left(\frac{y_o}{w}\right)^{b_1} (DRF)^{c_1}\right]^{1.5}}{w^{-0.5}\sqrt{2(y_o - y_t)}} \tag{7}$$

$$DRF = \frac{\frac{(y_o - y_t)}{w}}{\frac{\lambda(y_t - y_2)}{w} + \frac{(y_o - y_t)}{w}} \tag{8}$$

Where: C_d; is the discharge coefficient, y_o; is the upstream water depth, w; is the gate opening, y_t; is the tailwater depth, y_2; is the subcritical sequent depth, and DRF; is the discharge reduction factor, λ is a constant parameter = 1.033, and a_1, b_1, and c_1 are numerical constants obtained throughout experimental data as follows:

$a_1 = 0.655$, $b_1 = 0.407$, and $c_1 = 0.219$.

Bijankhan and Kouchakzadeh (2015) experimentally studied the hydraulics of flow across parallel sluice gates under minimum flow conditions, considering different operation schemes in symmetrical or asymmetrical gate installations. A formula has been developed to describe the flow passed through operated gates (free, submerged, and transitional conditions). Sauida (2014) conducted an experimental model to investigate and empirically validate the various variables influencing the outflow discharge through submerged multiple sluice gates (i.e., gates operational management, and expansion ratios). The author developed Eq. (9) to estimate the discharge coefficient C_d for the sluice gate model.

$$C_d = F\left(\frac{H_u}{G}\right)^{0.026}\left(\frac{y_t}{G}\right)^{0.17}\left(\frac{H_u - y_t}{G}\right)^{-0.04}(e)^{0.137} \tag{9}$$

Where: F; is constant equal to 0.465 for symmetric operation, and 0.48 for asymmetric operation, H_u; is the upstream water depth, y_t; is the tailwater depth at the end of the jump, G; is the gate opening height, and e; is the expansion ratio.

Focusing on the expansion ratio in open channel, it is defined as the ratio between two cross sections at which the canal width was widened.

Different contraction coefficient calculations were presented based on the shape of a radial gate leaf using the (E-M) principle; Shayan et al. (2014). The outcomes concluded that the contraction coefficient decreases as the gate leaf angle and the gate opening increase. The contraction coefficient was independent based on the stage of submergence. Equations (10) and (11) were deduced for calculating the contraction coefficient, δ and discharge coefficient, C_d, respectively, as follows:

$$\delta_{(sharp)} = 0.115\theta_r^{-1.89} - 0.236a^{0.226} + 0.755 \tag{10}$$

Where: a; is empirical constant = 0.512, and θ_r; is the gate leaf angle (in radians).

$$C_d = C_c\sqrt{\frac{1 - s}{1 - C_c^2\, a^2}} \tag{11}$$

Where: s = relative submergence, $\frac{y_2}{H_u}$; a = relative gate opening, $\frac{w}{H_u}$; and C_c; is the contraction coefficient.

Abdelhaleem (2017) experimentally studied the sill installation under submerged radial gates on the flow characteristics and the local scour directly downstream stilling basin. The results indicate that using radial gates without a sill was more effective compared to utilizing a sill. Equation (12) was deduced to calculate the critical water depth under submerged flow through radial gates with a sill.

$$\frac{y_c}{w} = a_2\left(\frac{y_o}{w}\right)^{b_2}\left(\frac{z}{w}\right)^{c_2}(DRF)^{d_2} \tag{12}$$

Where: y_o; is the upstream water depth, z; is the sill height, DRF; is the discharge reduction factor was calculated from Eq. (8), at which the values of λ, a_2, b_2, c_3, and d_2 are constants calculated from the experimental data as follows:

$\lambda = 1.138$, $a_2 = 0.819$, $b_2 = 0.312$, $c_2 = 0.023$, and $d_2 = 0.314$.

Abdelhaleem (2017) developed Eq. (13) for calculating the relative length of the submerged jump, $\frac{L_j}{y_1}$.

$$\frac{L_j}{y_1} = 13.19F_1^{0.97}S^{0.47} \tag{13}$$

Where: F_1; is the initial Froude number at vena contracta, y_1; is the water depth at vena contracta (minimum jet thickness), and S; is the submergence ratio.

Rahman et al. (2020) used the collected data from experimental model on radial gates to simplify the discharge calculations without compromising accuracy. Two empirical equations were deduced for the discharge coefficient for free and submerged flow. Babaei et al. (2021) used a hybrid technique by integrating experimental and analytical work to investigate the influence of a quarter-circular gate on the flow characteristics and discharge coefficient. The results demonstrated that the flow depth and the velocity profile were uniform downstream of the quarter-circular gate, and no contraction section was observed. Furthermore, the discharge coefficient of the quarter-circular gate was found to be larger, taking into consideration the sluice and radial gates. Guo et al. (2021) used experimental work supported by prototype measurements to study the discharge calibration method. The accuracy of the predicted discharges was acceptable. Shayan et al. (2021) applied the Energy and Momentum (E-M) principle to predict theoretical-based equations for estimating the flow discharge passed from radial gate under free and submerged flow conditions. Laishram et al. (2022) conducted experimental work to compare the hydraulic jump characteristics downstream (radial gate and sluice gate). The study of energy dissipation was included. The results highlight the radial gate superior sluice gate based on the structural safety, flexibility of flow control, in addition to dissipating the flow energy.

The artificial intelligence, AI was also incorporated in studying the hydraulics of radial gates. Tao et al. (2022) integrated three different machine learning, ML models to predict the discharge coefficient for both free and submerged flow downstream radial gates. The outcomes showed acceptable predictions. Moreover, the accuracy of the predicted model was higher for free flow conditions compared to the submerged flow. Yaseen et al. (2023) developed advanced intelligence models for radial gates to predict the discharge coefficient under free and submerged flow conditions. Hosny et al. (2025) used ML model to predict the discharge coefficient, $C_{d,}$ for both radial gate and sluice gate using two distinct gate types under submerged flow conditions.

The research gap is that while studies have been done on the hydraulic flow characteristics of single and multiple sluice gates, there is a significant lack of experimental work on the impact of multi-radial gates and their operational management, specifically under symmetric and asymmetric flow regimes.

Therefore, the study is motivated to address this by experimentally exploring the performance of a new proposed operational barrage regime using multi-radial gates under different flow conditions.

2. Dimensional analysis

The hydraulic and geometrical parameters affecting the flow characteristics at different radial gate operation schemes are described in the following functional form:

$$f\left(B, H_u, y_t, Q, b, \theta, w, L_j, N, v, c_d, y_1, y_2, S_o, g, \rho, \mu, \sigma, \delta\right) = 0 \tag{14}$$

In which: B; the flume width, H_u; the upstream water depth, y_t; the tailwater depth, Q; the flow discharge, b; the gate width, θ; the gate leaf angle, w; the gate opening, L_j; the length of submerged jump, N; the number of opened gates, v; the flow velocity, C_d; the discharge coefficient, y_1; the initial water depth that located at vena contracta, y_2; the backup water depth, g; the gravitational acceleration, S_o; the bed slope, ρ; the water density, μ; the dynamic water viscosity, σ; the surface tension, δ; the contraction coefficient. The study variables are presented in Figure 1.

Some of these variables are unchanged throughout the experimental work, for example, the gravitational acceleration, g, and for the flume geometry, e.g., B, b, and S_o. Other variables are found to have insignificant influence, e.g., ρ, σ, and μ, for example, due to the gravitational flow type. Consequently, the constant parameters and the variables of minor effects may be excluded from the initial equation to include only the effective terms.

Using Buckingham's π-theorem and applying the characteristics of dimensional analysis yields;

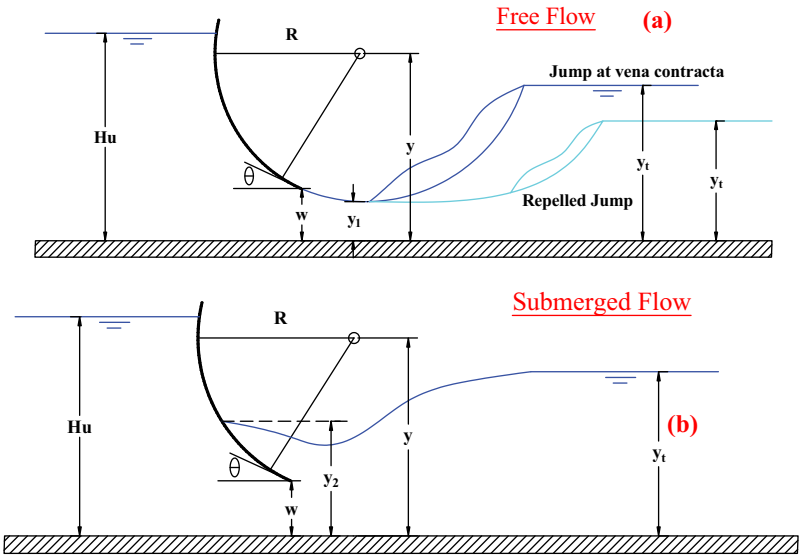

Figure 1. Definition sketch for hydraulic characteristics of radial gate: (a) free flow; (b) submerged flow.

$$f\left(\frac{H_u}{w},\frac{y_t}{w},\frac{y_1}{w},\frac{L_j}{y_1},c_d,\theta,\frac{\rho Q}{B\mu},\frac{v}{\sqrt{gy_1}},\frac{B}{N*w},\frac{y_t-y_2}{y_2}\frac{\rho v^2 B}{\sigma},\delta\right)=0 \tag{15}$$

Where;$\frac{v}{\sqrt{gy}}$ is the Froude number, Fr_1; $\frac{\rho\, Q}{B\mu}$ is the Reynolds number, R_e; $\frac{\rho v^2 B}{\sigma}$ is the Weber number, W_e; $\frac{yt-y2}{y2}$ is the submergence ratio, S; and $\frac{B}{N*w}$ is the expansion ratio, e; substitute in Eq (16);

$$f\left(\frac{H_u}{w},\frac{y_t}{w},\frac{y_1}{w},\frac{L_j}{y_1},C_d,\theta,R_e,Fr_1,e,s,w_e,\delta\right)=0 \tag{16}$$

The flow just downstream radial gate is supercritical and gradually turned to subcritical away from the tested region. The calculations of Reynolds No. (Re) were carried out at the location where the minimum water depth is measured. The Reynolds No. values ranged from 2425 to 15,913, which are greater than 2000, to emphasize that the flow downstream of the examined radial gates is completely turbulent. Whereas the open channel flow is mainly gravitational, the influence of viscosity and surface tension is of minor importance.

In the case of the tested fluid is water, the variation in dynamic viscosity is extremely small; Therefore, the effect of Reynolds and Weber numbers can be ignored due to their insignificant impact.

Considering the constants and variables of minor effect, Eq (16) was justified to deduce Eq (17) as follows:

$$f\left(\frac{H_u}{w},\frac{y_t}{w},\frac{y_1}{w},\frac{L_j}{y_1},c_d,\theta,Fr_1,e,s,\delta\right)=0 \tag{17}$$

3. Experimental setup and procedures

The experimental work is located at the hydraulic laboratory of the Hydraulics Research Institute (HRI), National Water Research Center (NWRC), Egypt. A 2-D flume model was utilized to study the impact of radial gates' operational management on the hydraulic flow characteristics. The flume dimensions are 15.3 m long, 1.75 m wide, and 0.45 m deep. The floor of the flume model is made of concrete, and part of the side walls are made of bricks covered by mortar to prevent leakage. The other part is made of Plexiglas to allow visual investigations, measurements, and photography of the flow pattern. Figure 2 shows a definition sketch for the used flume. The screen box filled with large gravel mentioned in Figure 2 is mainly installed to generate uniform flow by scattering the excess energy created by the effect of the lifting pump at the flume entrance.

The water depth downstream of the control structure is adjusted by a tailgate fixed at the flume end. The water is supplied from a head tank. A centrifugal pump with 100 l/s as maximum flow discharge conveys the water from the sump to the reservoir, where it flows through the flume. The flume inlet consists of

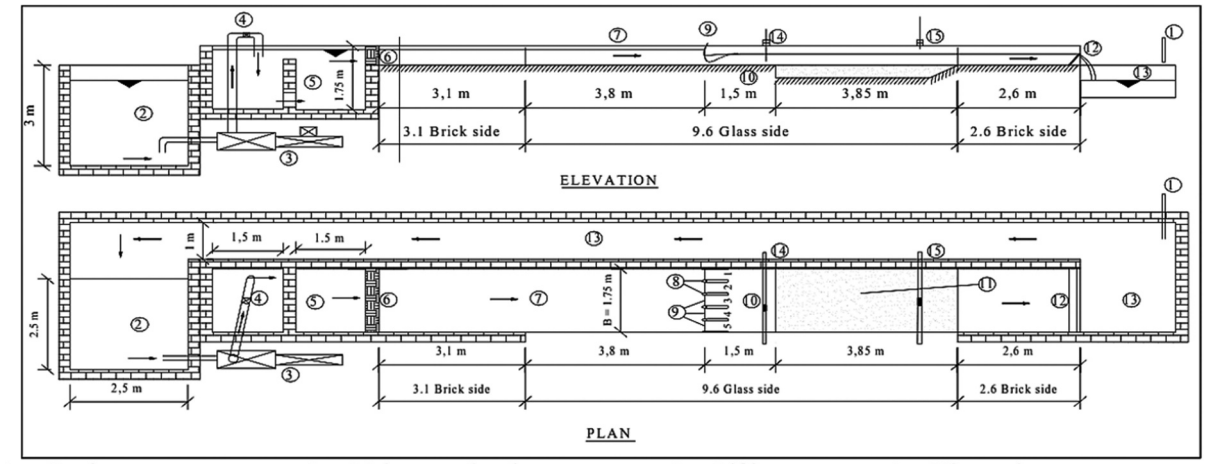

1- Fresh water source 2- Main ground tank 3- Lifting pump 4- Ultrasonic meter
5- Secondary tank 6- Screen box filled with gravel 7- Main channel 8- Piers
9- Radial gates 10- Solid floor 11- The mobile bed 12- The tail gate
13- By-pass channel 14- Electro-Magnetic Current meter 15- Point gauge

Figure 2. Definition sketch for the used flume.

a masonry basin of 2.50 m length, 2.50 m width, and 3.0 m depth. The flow is transmitted through a screen box filled with large gravel, followed by another screen box filled with 2-in. diameter plastic pipes located at the flume inlet to dissipate water energy and scatter any excess turbulence.

The simulated structure is located 6.90 m downstream of the flume inlet. The simulated model consists of five vents controlled by radial gates with 0.45 m radius, a gate opening width of 0.286 m, 0.07 m pier width, and two side half piers of 0.02 m width; Figure 3.

The dimensions of the constructed regulator in Figure 3 were selected to simulate the flow across the New El-Tawfiki Regulator, the El-Salhya Regulator, and the left part of the spillway of New Assiut barrage with different scales, which is located in Egypt.

The model test program was prepared carefully to study the effect of the selected independent parameters: flow discharge, Q; tailwater depth, y_t; number of opened gates, N; and the opened gates arrangement, as presented in Table 1.

Eighty experimental runs considering five different gate arrangements under 16 different flow conditions were done. The operation schemes were divided into four scenarios for symmetric conditions and one for asymmetric conditions. Each operation scheme was operated under 16 hydraulic flow conditions, considering four flow discharges, Q = 26, 29, 32, and 35 l/s, and four tailwater depths y_t = 0.21, 0.23, 0.25, and 0.27 m. The upstream water depth was constant during experiments, H_u = 0.40 m, and it was achieved experimentally through the adjustment of the gate opening.

The water depth associated with each flow discharge was adjusted using point gauge of accuracy ±0.1 mm. The flow discharge was measured using ultrasonic flowmeter with an accuracy of ±1.0% installed on the feeding pipe.

Regarding the experimental work procedure, firstly, the water-feeding source was opened; then, the water passed through the bypass channel until the water filled the main ground tank. The flow rate was measured by an ultrasonic flowmeter with an accuracy of ±1%. The lifting pump was activated to deliver the water from the main ground tank to the secondary tank. Once the secondary tank is filled with water, the lifting pump is turned-on with minimum operating capacity to fill the flume channel. The estimated gate opening was determined based on the operating conditions, including the specified flow discharge and the number of opened/closed gates in the test program. Upon activating the pump, the targeted discharge was conveyed through the gates, and the upstream water level was regulated by adjusting the gate openings accordingly. Subsequently, the downstream water level was controlled using the tailgate. The measurement starts once the flow reaches the steady state condition. The water depth measurements started just downstream of the simulated radial gates up to 2.0 m with 0.2 m interval

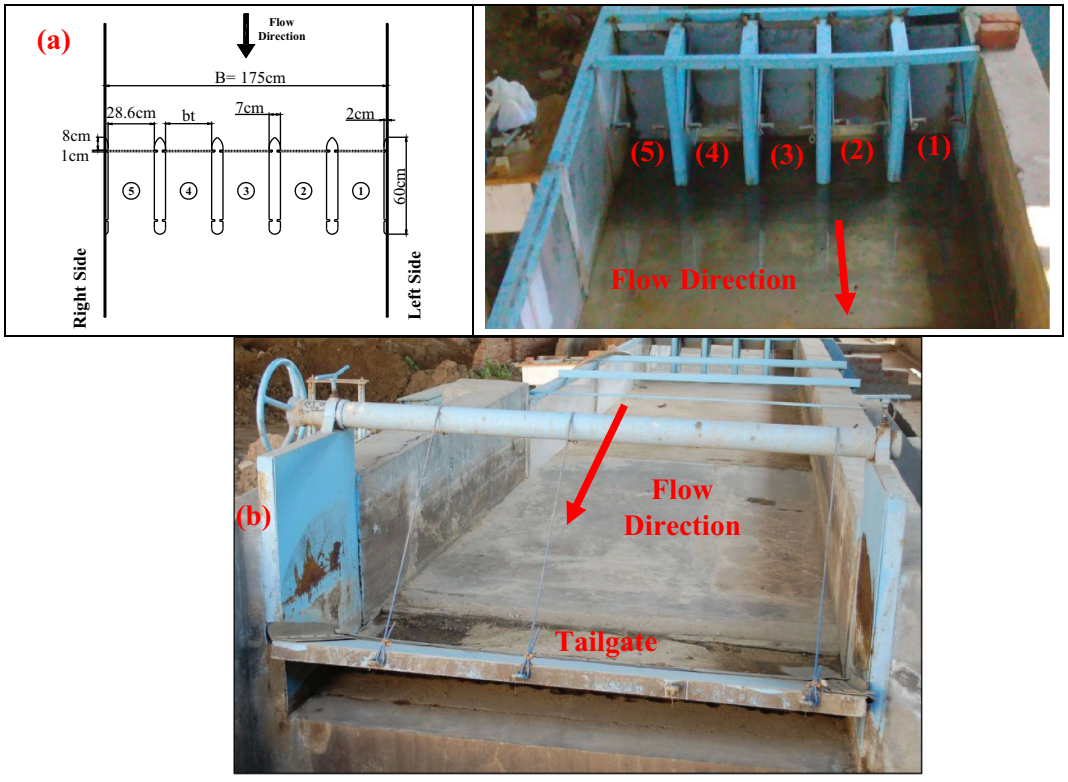

Figure 3. The simulated model: (a) sketch and photograph for the hydraulic control structure; (b) photograph for the tailgate installation.

along the flow direction. The previous steps were repeated for each test according to the scheme listed in Table 1.

4. Results and discussions

The recorded experimental results are presented, analyzed, and discussed in this section. The influence of the operation schemes of radial gates on the contraction and discharge coefficient, gate leaf angle, critical water depth, and length of hydraulic jump are explored. In addition, the distinguishing conditions considering submerged and free flow regimes are illustrated.

4.1. Distinguishing condition

Figure 4 presents the relation between relative upstream water depth, $\frac{H_u}{w}$ and relative tailwater depth, $\frac{y_t}{w}$. The figure explores the direct relationship between the investigated parameters, which confirms the stability of the control structure. The results of the experimental tests of all tested scenarios were compared to the data calculated by Bos (1989) formula Eq. (4). According to Bos (1989), the line presented in Figure 4 delineates the boundary between free and submerged-flow regimes. Accordingly, the observed results can be interpreted based on the position of the measured data with respect to this boundary. Data corresponding to $\frac{H_u}{w}$ values ranging from 5.41 to 5.71 fall within the free-flow region. Whereas data with $\frac{H_u}{w}$ values exceeding 5.71 lie above the borderline obtained by Eq. (4), indicating operation within the submerged-flow regime.

4.2. Influence of contraction coefficient, δ

Figures 5(a,b) explore the influence of the contraction coefficient, δ, on the radial gate leaf angle, θ, and the relative upstream water depth, $\frac{H_u}{w}$, respectively. The measured data are used to estimate the contraction coefficient using Eq. 1 developed by (Toch 1955) and compared to the outcomes from Eqs. 5, and 10

Table 1. The experimental test program.

Scenario No.	Test No.	Flow Discharge; Q (l/s)	Tailwater depth; Y_t (m)	No. of opened gates	Opened gates from Left side (looking D/S)					Symmetry
					1	2	3	4	5	
Scenario No. (1)	1	26	0.21	5	√	√	√	√	√	Symmetric
	2	26	0.23	5	√	√	√	√	√	Symmetric
	3	26	0.25	5	√	√	√	√	√	Symmetric
	4	26	0.27	5	√	√	√	√	√	Symmetric
	5	29	0.21	5	√	√	√	√	√	Symmetric
	6	29	0.23	5	√	√	√	√	√	Symmetric
	7	29	0.25	5	√	√	√	√	√	Symmetric
	8	29	0.27	5	√	√	√	√	√	Symmetric
	9	32	0.21	5	√	√	√	√	√	Symmetric
	10	32	0.23	5	√	√	√	√	√	Symmetric
	11	32	0.25	5	√	√	√	√	√	Symmetric
	12	32	0.27	5	√	√	√	√	√	Symmetric
	13	35	0.21	5	√	√	√	√	√	Symmetric
	14	35	0.23	5	√	√	√	√	√	Symmetric
	15	35	0.25	5	√	√	√	√	√	Symmetric
	16	35	0.27	5	√	√	√	√	√	Symmetric
Scenario No. (2)	17	26	0.21	3	–	√	√	√	–	Symmetric
	18	26	0.23	3	–	√	√	√	–	Symmetric
	19	26	0.25	3	–	√	√	√	–	Symmetric
	20	26	0.27	3	–	√	√	√	–	Symmetric
	21	29	0.21	3	–	√	√	√	–	Symmetric
	22	29	0.23	3	–	√	√	√	–	Symmetric
	23	29	0.25	3	–	√	√	√	–	Symmetric
	24	29	0.27	3	–	√	√	√	–	Symmetric
	25	32	0.21	3	–	√	√	√	–	Symmetric
	26	32	0.23	3	–	√	√	√	–	Symmetric
	27	32	0.25	3	–	√	√	√	–	Symmetric
	28	32	0.27	3	–	√	√	√	–	Symmetric
	29	35	0.21	3	–	√	√	√	–	Symmetric
	30	35	0.23	3	–	√	√	√	–	Symmetric
	31	35	0.25	3	–	√	√	√	–	Symmetric
	32	35	0.27	3	–	√	√	√	–	Symmetric
Scenario No. (3)	33	26	0.21	2	–	√	–	√	–	Symmetric
	34	26	0.23	2	–	√	–	√	–	Symmetric
	35	26	0.25	2	–	√	–	√	–	Symmetric
	36	26	0.27	2	–	√	–	√	–	Symmetric
	37	29	0.21	2	–	√	–	√	–	Symmetric
	38	29	0.23	2	–	√	–	√	–	Symmetric
	39	29	0.25	2	–	√	–	√	–	Symmetric
	40	29	0.27	2	–	√	–	√	–	Symmetric
	41	32	0.21	2	–	√	–	√	–	Symmetric
	42	32	0.23	2	–	√	–	√	–	Symmetric
	43	32	0.25	2	–	√	–	√	–	Symmetric
	44	32	0.27	2	–	√	–	√	–	Symmetric
	45	35	0.21	2	–	√	–	√	–	Symmetric
	46	35	0.23	2	–	√	–	√	–	Symmetric
	47	35	0.25	2	–	√	–	√	–	Symmetric
	48	35	0.27	2	–	√	–	√	–	Symmetric
Scenario No. (4)	49	26	0.21	1	–	–	√	–	–	Symmetric
	50	26	0.23	1	–	–	√	–	–	Symmetric
	51	26	0.25	1	–	–	√	–	–	Symmetric
	52	26	0.27	1	–	–	√	–	–	Symmetric
	53	29	0.21	1	–	–	√	–	–	Symmetric
	54	29	0.23	1	–	–	√	–	–	Symmetric
	55	29	0.25	1	–	–	√	–	–	Symmetric
	56	29	0.27	1	–	–	√	–	–	Symmetric
	57	32	0.21	1	–	–	√	–	–	Symmetric
	58	32	0.23	1	–	–	√	–	–	Symmetric
	59	32	0.25	1	–	–	√	–	–	Symmetric
	60	32	0.27	1	–	–	√	–	–	Symmetric
	61	35	0.21	1	–	–	√	–	–	Symmetric
	62	35	0.23	1	–	–	√	–	–	Symmetric
	63	35	0.25	1	–	–	√	–	–	Symmetric
	64	35	0.27	1	–	–	√	–	–	Symmetric

(*Continued*)

Table 1. (Continued).

Scenario No.	Test No.	Flow Discharge; Q (l/s)	Tailwater depth; Y_t (m)	No. of opened gates	Opened gates from Left side (looking D/S)					Symmetry
					1	2	3	4	5	
Scenario No. (5)	65	26	0.21	1	–	–	–	–	√	Asymmetric
	66	26	0.23	1	–	–	–	–	√	Asymmetric
	67	26	0.25	1	–	–	–	–	√	Asymmetric
	68	26	0.27	1	–	–	–	–	√	Asymmetric
	69	29	0.21	1	–	–	–	–	√	Asymmetric
	70	29	0.23	1	–	–	–	–	√	Asymmetric
	71	29	0.25	1	–	–	–	–	√	Asymmetric
	72	29	0.27	1	–	–	–	–	√	Asymmetric
	73	32	0.21	1	–	–	–	–	√	Asymmetric
	74	32	0.23	1	–	–	–	–	√	Asymmetric
	75	32	0.25	1	–	–	–	–	√	Asymmetric
	76	32	0.27	1	–	–	–	–	√	Asymmetric
	77	35	0.21	1	–	–	–	–	√	Asymmetric
	78	35	0.23	1	–	–	–	–	√	Asymmetric
	79	35	0.25	1	–	–	–	–	√	Asymmetric
	80	35	0.27	1	–	–	–	–	√	Asymmetric

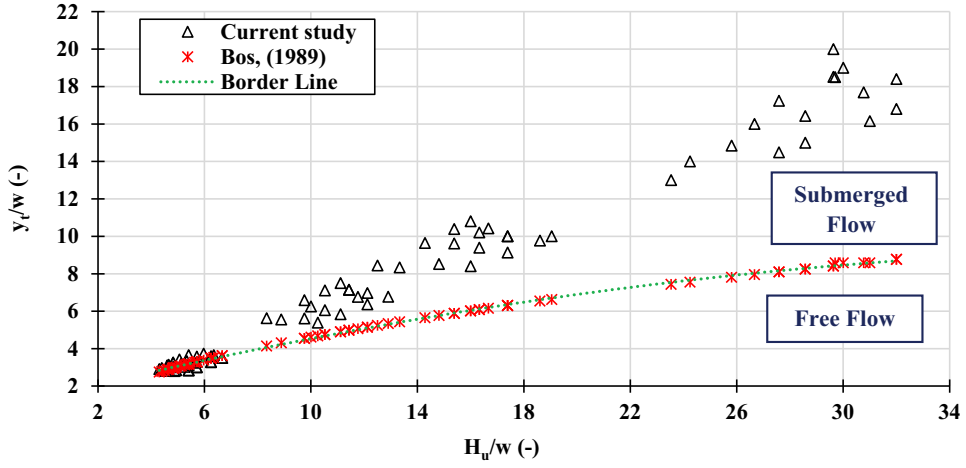

Figure 4. The distinguishing condition curve.

developed by (Tel 2000); and (Shayan et al. 2014), respectively. The data used in Figure 5(a,b) are plotted using all tested conditions.

Figure 5(a) illustrates that the contraction coefficient decreases with the increase in the gate leaf angle, θ, which is a function of the gate opening height. The recorded measurements are compared to the corresponding values reported by Shayan et al. (2014). The findings are in good agreement with the previous studies, where similar trend lines are noticed. The discrepancy between the contraction coefficient, δ, observed in the present study and the values calculated by Tel's (2000) data decreased as the gate leaf angle, θ, increased. Emphasizing the current study measurements, the figure shows that the values of the contraction coefficient ranged between 0.633 and 0.659, with gate leaf angle that ranged between 60.44 and 71.61.

Figure 5(b) demonstrates that the contraction coefficient, δ, is directly proportional to the relative upstream water depth $\frac{H_u}{w}$. The study outcomes show good agreement with the findings of Shayan et al. (2014), where a similar trend is remarked. Furthermore, the disparity observed in the data aligns with the differences calculated using the equations developed by Tel (2000) and Toch (1955). The recorded differences resulted in changes in flow characteristics and boundary conditions.

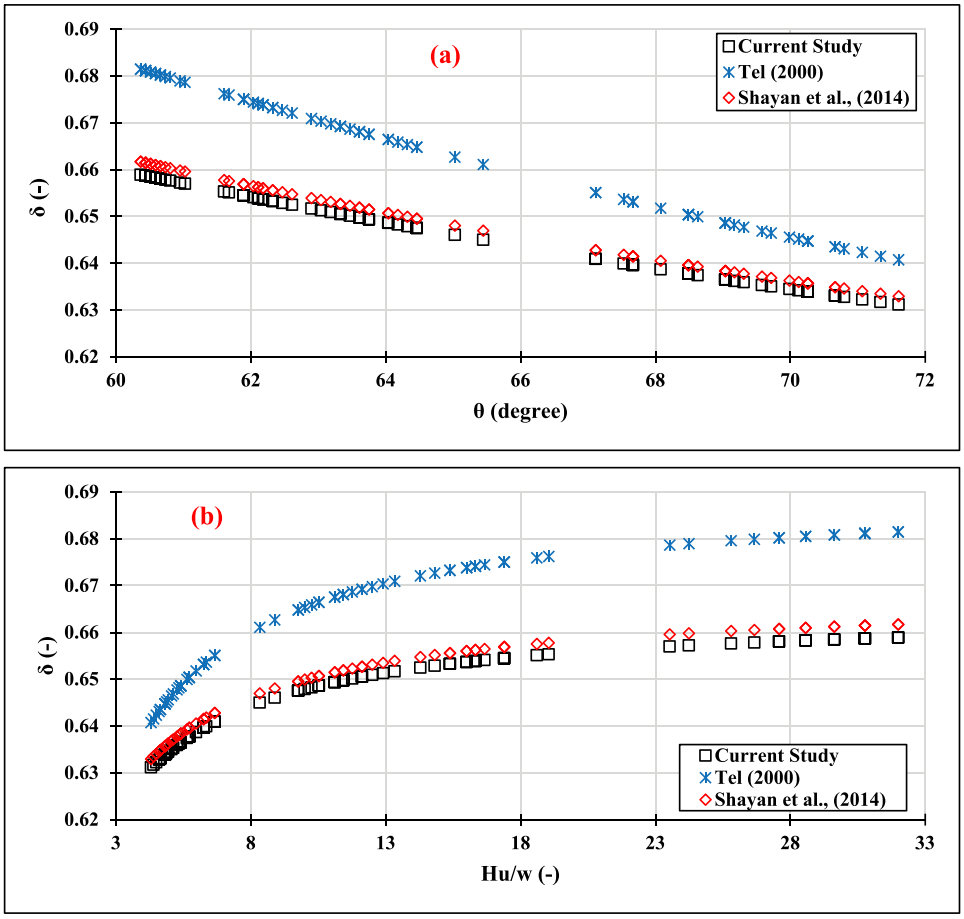

Figure 5. Submerged radial gate contraction coefficient, δ, as a function of: (a) θ and (b) $\frac{H_u}{w}$.

4.3. *Influence of discharge coefficient, C_d*

Figure 6 illustrates the relation between the discharge coefficient, C_d and the relative upstream water depth, $\frac{H_u}{w}$ taking into account the expansion ratio, e; the relative tailwater depth, $\frac{y_t}{w}$ and the initial Froude No., Fr_1. Figure 6 is plotted for the carried-out test program.

Figure 6(a) shows the relation between the discharge coefficient, C_d, and $\frac{H_u}{w}$ with expansion ratio, e ranging from 1.22 to 6.12. However, to distinguish between the symmetric and asymmetric operations, only e = 6.12 is presented, because it refers to the critical scenario, where only one gate is activated to pass the flow discharge. The discharge coefficient and expansion ratio were calculated using Eqs. (2) and (3).

The figure demonstrates that the expansion ratio decreases with the increase in upstream water depth. In addition, there is no significant effect of the operated gates arrangement in the expansion ratio, resulting from the effect of the total width of the opened gates. Also, the C_d is increased by the increase in $\frac{H_u}{w}$ resulting in noticeable improvement in pressure distribution, reducing the flow separation, better approach flow conditions, increasing the gate submergence, and a more uniform velocity distribution. As a result, a remarkable increase in the flow efficiency and, consequently, a higher discharge coefficient. Also, the figure highlights that the increase in discharge coefficient is slight with the higher expansion ratio; on the contrary, it is found significant for the small expansion ratio.

Figure 6(b) illustrates that by focusing on the effect of the relative tailwater depth, $\frac{y_t}{w}$; it is noticed that $\frac{y_t}{w}$ is directly proportional to relative upstream water depth, $\frac{H_u}{w}$. These findings explore the good consistency with the data reported in sub-section 4.1. The dimensionless tailwater depth ranged from 2.80 to 19.23, depending on the number of opened gates. The relative tailwater depth is directly proportional to the number of activated gates and inversely proportional to the gate opening. The discharge coefficient is

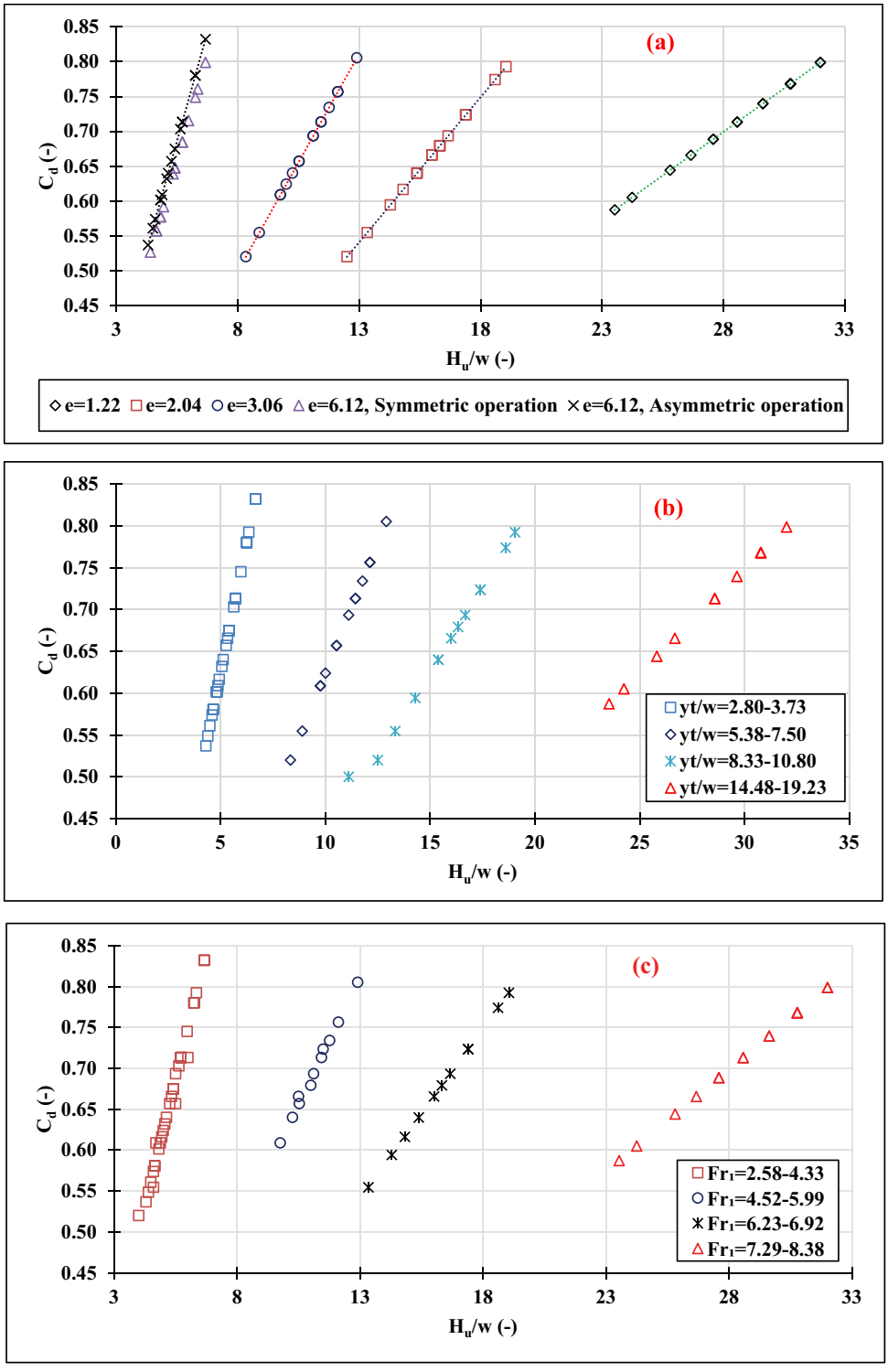

Figure 6. Variation in C_d against $\frac{H_u}{w}$ for different: (a) e; (b) $\frac{y_t}{w}$, (c) Fr_1.

increased for each selected range by the increase in flow discharge and the decrease of both gate opening and the total width of opened gates. The recorded outcomes are consistence with Eq. (2).

Figure 6(c) shows that the initial Froude No., Fr_1, increases with the increase in relative upstream water depth and is inversely proportional to gate opening, which is considered the dominant factor of initial water depth. The Fr_1 ranged between 2.58 and 8.38 was divided into four categories depending on the operation scheme. The tested groups of Fr_1 show a similar trend and vary in the slope of best best-fit line. The smaller

group range shows a steeper slope. The discharge coefficient, $C_{d,}$ increases with the increase in Froude No., Fr_1 for the operated scenario.

To define the influence of gate type on the C_d under different flow conditions, including symmetric and asymmetric operations, Figure 7 is plotted. Two shapes of gates are presented: sluice and radial types. The C_d for the radial gate model is calculated using the measured experimental values. However, the C_d for the sluice gate model is calculated using Eq. (9) developed by Sauida (2014). Equation (9) is selected because it is derived for similar hydraulic conditions relative to the current study. A similar trend line is noticed for the experimental data and the outcomes of Eq. (9) by Sauida (2014). The presented data in Figure 7 is for e = 6.12, which is selected to represent the critical case corresponding to operating only one gate.

The figure shows that the discharge coefficient, C_d, calculated for asymmetric radial gates is higher than for symmetric radial gates by 4.0% to 4.2% with the best fit-line slope ranging between 12.00% and 12.44%. Noticeable reduction in the discharge coefficient is found for the instance of the sluice gate, ranging between 2.1% and 3.9% and the best fit-line slope ranged between 1.28% and 1.88%. The figure outcomes that the sluice gate have superiority compared to the radial gatesfor instance, of $\frac{H_u}{w}$ less than 6.25. In addition, the asymmetric gate operation is more efficient than the symmetric gate operation for both sluice and radial gates.

The total number of experimental works is 80 test runs, 65 of them were implemented in multi-regression analysis model to develop Eq. (18) as a simple empirical equation to predict the discharge coefficient, C_d for limited, similar flow conditions. Out of date used in equation development (i.e., the rest measurements of 15 runs) were used for the validation:

$$C_d = a\left(\frac{H_u}{w}\right) + b(Fr_1) + c(e) + d(S) + f(\theta) + h \tag{18}$$

Where; a = 0.0231, b = −0.0915, c = 0.1247, d = −0.1015, f = −0.078, and h = 5.5457
The coefficient of determination, $R^2 = 0.899$
Standard Error of the Estimate, SEE = 0.0255.

It should be mentioned that only the effective parameters of major dependent correlation with the C_d are involved in Eq. (18). There are other variables presented in Eq (17), but they are excluded due to insignificant impact on the C_d and to avoid complexity in application.

Investigating Eq. (18), it is noticed that the C_d is directly proportional to $\frac{H_u}{w}$ and the expansion ratio, e, and inversely proportional to the Froude No., Fr_1; the submergence ratio, S; and the gate leaf angle, θ. These findings are in good agreement with the analysis of sub-section 4.3 that describes the relation between C_d and ($\frac{H_u}{w}$, e).

To check the accuracy of the developed equation, the calculated values are compared to other formulas developed by (Bijankhan et al. 2013; Sauida 2014; Shayan et al. 2014; Abdelhaleem 2017). The outcomes are presented in Figure 8.

The measured discharge coefficient, C_d, ranges from 0.52 to 0.83, which covers the values of calculated data from other comparable equations. Figure 8 exhibits a significant contrast between the developed formula Eq. (18) and Sauida's (2014). The differences are resulted in multi-gate operation. The data obtained from applications of other formulas have similar trend line to the measured data, with minor variations in values.

From a statistical view, to explore the reliability of Eq. (18), the evaluation indicator Root Mean Square Error, RMSE was applied to find the differences between the results of the discharge coefficient, C_d, due to applying the developed equation and other formulas considered in Figure 8. The evaluation indicator is expressed as follows:

$$RMSE = \sqrt{\frac{1}{n}\sum_{i=1}^{n}(Cd_m - Cd_C)^2} \tag{19}$$

The Root Mean Square Error, RMSE, ranged between 0.029 and 0.063 for different equations. But the RMSE = 0.011 when comparing measured data to the developed equations. The results of RMSE

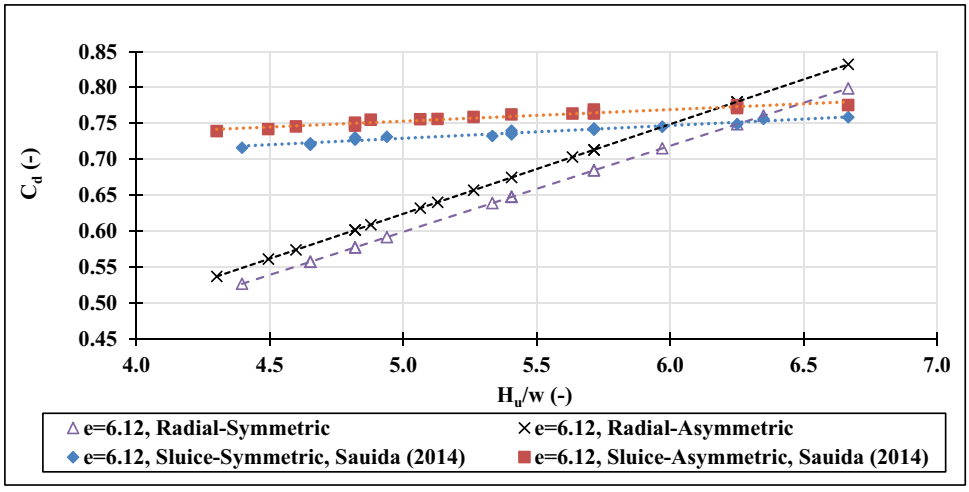

Figure 7. Effect of gate shape and type of operation on the C_d.

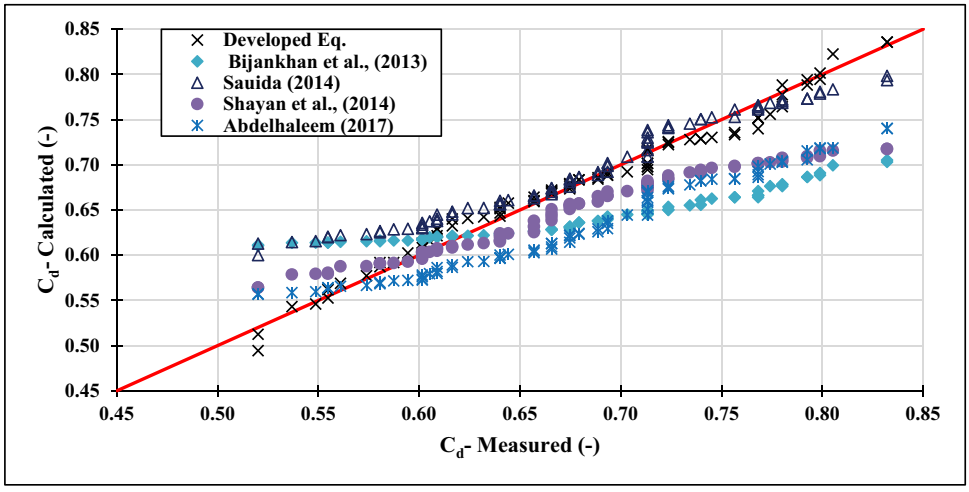

Figure 8. Comparison between measured and calculated discharge coefficients, C_d.

are less than 10, which demonstrates the sufficient quality of the measured data and the developed equations.

4.4. Influence of gate leaf angle, θ

To explore the influence of the gate leaf angle, θ, on the flow pattern Figure 9 is plotted. Figure 9 shows the relation between relative upstream water depth, $\frac{H_u}{w}$ and tailwater depth, $\frac{y_t}{w}$ based on the gate leaf angle. Equation 6 was used to calculate the gate leaf angle. From figure investigations, it is illustrated that the gate leaf angle, θ, is increased by the increase in the gate opening, w, and decreased by the increase in the relative tailwater depth, $\frac{y_t}{w}$.

The figure defines the linearity of all plotted trend lines for the tested gate leaf angle. The trend lines' slope decreases with the increase in gate leaf angle. Furthermore, the gate leaf angle and the gate opening are found increased in sequence. The increase in gate leaf angle resulting in minimizing the functional operated gates used to convey similar flow discharge. Consequently, affecting the operational efficiency of the radial gates.

Using radial gates with low values of gate leaf angle covers wider range of relative upstream and downstream water depths, in contrast to high values of, θ. So, using gates with lower gate leaf angles is more functional compared to the higher ones.

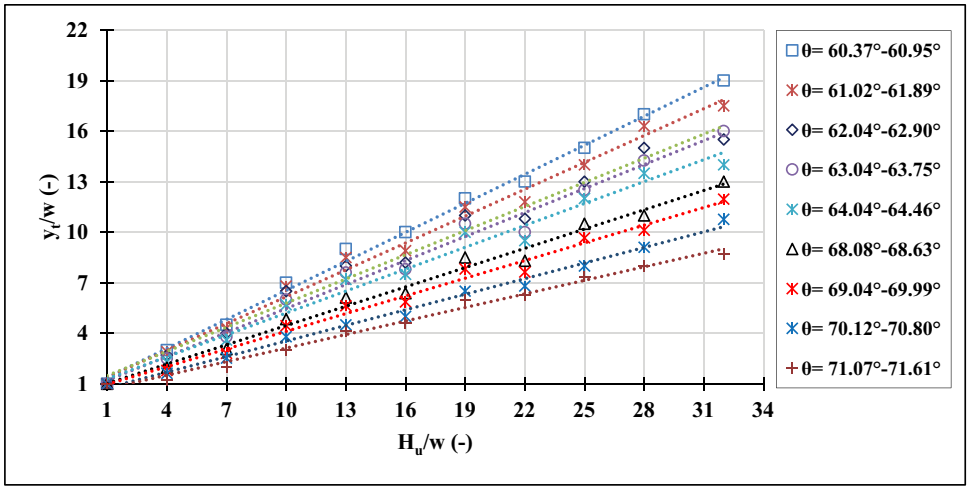

Figure 9. Relation between $\frac{y_t}{w}$ and $\frac{H_u}{w}$ for different gate leaf angles, θ.

4.5. The critical water depth, y_c

Figure 10 presents the relation between relative critical water depth, $\frac{y_c}{w}$ and relative upstream water depth, $\frac{H_u}{w}$. Also, the figure shows a comparison between the experimental measurements and the outcomes by applying Eq. (12). Noting that, during the applications of Eq. (12), the sill height is considered by zero to be consistent with the current work, where the tests were run on an apron without sill. The figure explores the relation between $\frac{y_c}{w}$ and $\frac{H_u}{w}$ is in direct proportion to convey the higher discharge associated with the increased upstream head to avoid flow spilling out. Consequently, noticeable increase in the critical depth. The values of $\frac{y_c}{w}$ are ranged between 2.49 and 9.83. Also, under fixed upstream water depth, the critical water depth is inversely proportional to the number of operated gates and in direct proportion to gate opening.

Regarding the measurement accuracy, the experimental and calculated data are in good agreement, where the percentage of error was around under estimation of ±3%.

Equation (20) was developed from the measured data to estimate $\frac{y_c}{w}$ as follows:

$$\frac{y_c}{w} = -0.002693\left(\frac{H_u}{w}\right)^2 + 0.362\left(\frac{H_u}{w}\right) + 1.089 \tag{20}$$

The coefficient of determination, $R^2 = 0.9968$.

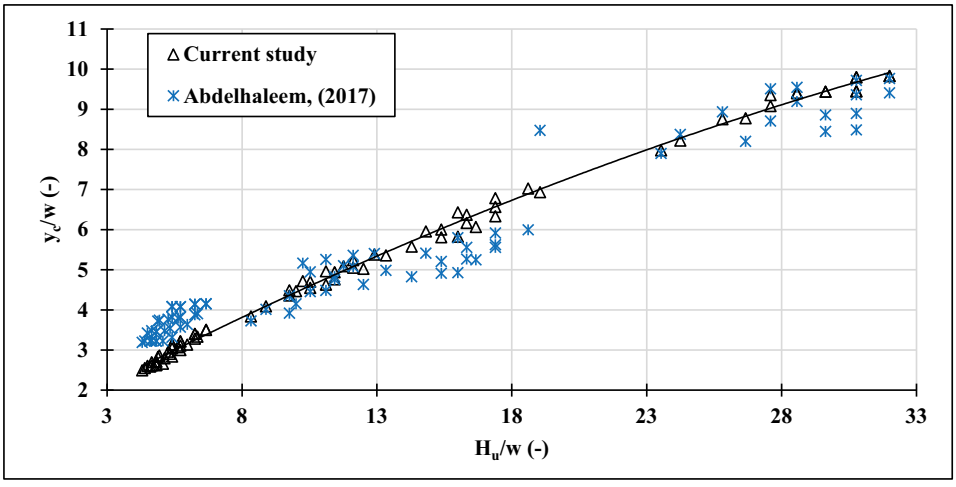

Figure 10. Comparison between measured $\frac{y_c}{w}$ and previous formulas.

To check the statistical accuracy of the developed empirical equation, the Root Mean Square Error, RMSE, between Eq. (12) and Eq. (20) are calculated and found equal to 0.6799, which ensures the equation's accuracy.

4.6. *Influence of length of hydraulic jump, L_j*

Figure 11(a,b) present the variation in the relative length of the submerged jump, $\frac{L_j}{w}$ against the initial Froude No., Fr_1, considering different expansion ratios, e, and the gate leaf angles, θ, respectively. Figure 11a demonstrates that the expansion ratio is inversely proportional to the $\frac{L_j}{w}$, and Fr_1. These findings are due to that the expansion ratio is affected by the number of operated gates. In other words, activating five operational gates leads to a decrease in the gate opening that, in turn, increases the velocity. Thus, noticeable increases in the initial Froude No. and the length of the submerged jump. The opened gates symmetry shows insignificant influence with $\frac{L_j}{w}$. Exploring Figure 11b, it could be observed that the submerged jump length increases as the gate leaf angle decreases. These findings are in good consistent with the discussion in sub-section 4.4. As the lower gate leaf angle corresponds to the maximum number of operated gates, it reversely affects the Froude No. and the relative length of the submerged jump.

Figure 12 discusses the functional relation between the measured relative length of the submerged hydraulic jump $\frac{L_j}{y_1}$ and the calculated by applying Eq. (13). Noting that the total number of experimental tested runs are 80, out of them 65 are employed to derive Eq. (21) that predicts the relative length of

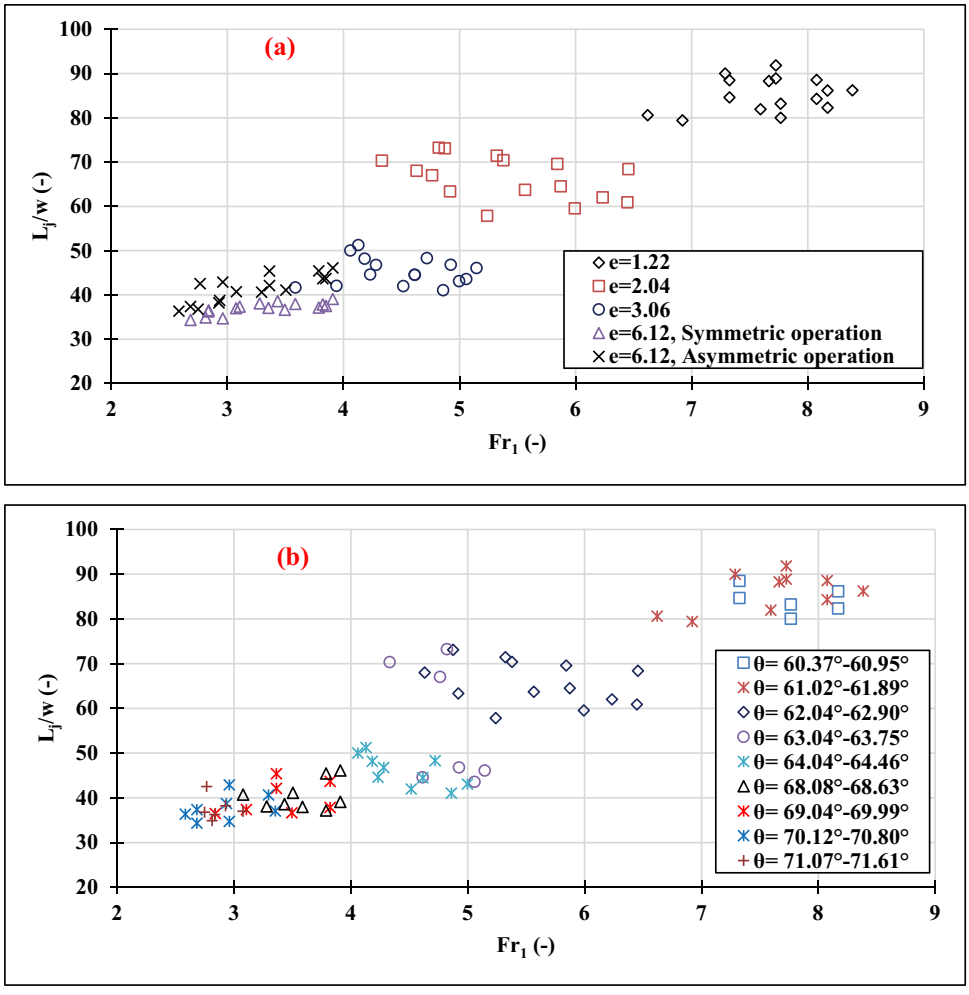

Figure 11. Relation between $\frac{L_j}{w}$ and Fr_1 for different: (a) expansion ratios, e; (b) gate leaf angle, θ.

submerged hydraulic jump occurring downstream radial gates. The rest of the data was used to validate Eq. (21).

$$\frac{L_j}{y_1} = a\left(\frac{H_u}{w}\right) + b(Fr_1) + c(e) + d(S) + f(\theta) + h \tag{21}$$

Where: a = −2.5918, b = 22.4392, c = 1.578, d = 26.6672, f = 1.8574, and h = −169.51

The coefficient of multiple determination, $R^2 = 0.941$.

Standard Error of the Estimate, SEE = 5.25.

The developed equation is applicable for limited range of Froude No. ranged between 2.58 and 8.38.

The outcomes of measuring data, Eq. (13), and Eq. (21) are plotted in Figure 12. The evaluation indicator RMSE was used between the measured data and different Equations, and the value of RMSE ranged between 4.94 and 5.11 that demonstrates the high accuracy of the measured data and the good correlation with other equations. Also, similar trend between the tested parameters is found which implies a good correlation was observed between the measured and the predicted data.

Figure 13 presents the relation between the measured relative length of the submerged jump $\frac{L_j}{y_1}$ and the submergence ratio, S. The submergence ratio was calculated using Eq. (22).

$$S = \frac{y_t - y_2}{y_2} \tag{22}$$

The figure demonstrated that the submergence ratio increases as the relative length of the submerged hydraulic jump increases. It is reasoned by the increase in the head difference between the tailwater depth and the backup water depth.

For simplicity, a linear equation is developed from the measured data as shown below:

$$\frac{L_j}{y_1} = 25.816S + 26.679 \tag{23}$$

The coefficient of determination, $R^2 = 0.91$.

Focusing on the study limitation, the current experimental work outcomes and the associated derived empirical equations are applicable for single or multi-radial gates; however, the sluice gates are not employed. Regarding the flow conditions and operation schedule, this work has the flexibility to be applied for both free and submerged flow conditions, moreover, the symmetric and asymmetric gate operating

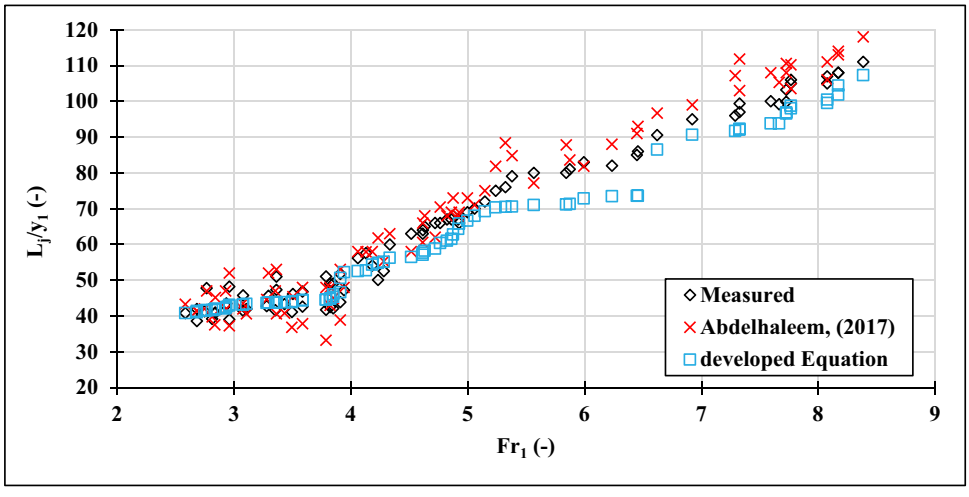

Figure 12. Comparison between measured, calculated, and previous formulas for $\frac{L_j}{y_1}$.

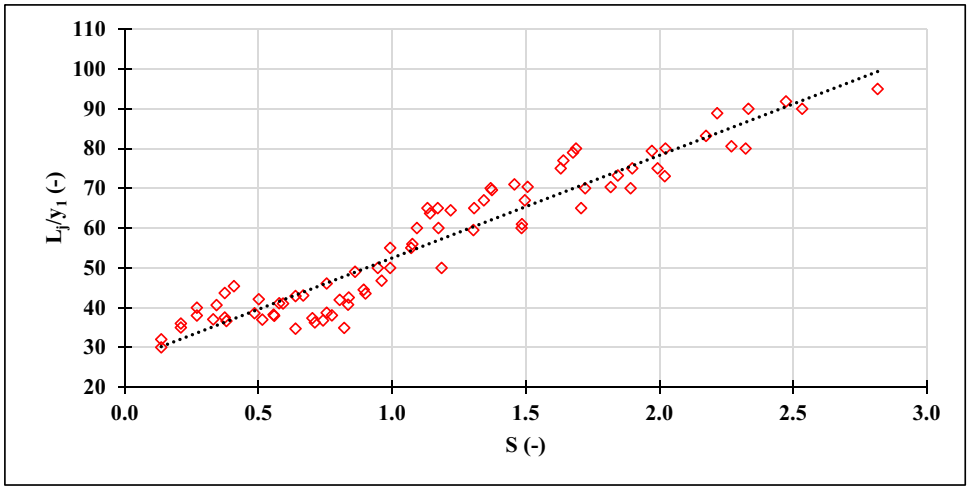

Figure 13. Relation between $\frac{L_j}{y_1}$ and the submergence ratio, S.

regimes. This study is limited for specific ranges of discharge and tailwater depths. The flow rate range is between 26 l/s and 35 l/s; however, the tailwater depth, y_t is ranged between 0.21 m and 0.27 m.

5. Conclusions

In the current study, an experimental model was used to assess the influence of operating schemes of radial gate arrangement. The investigations considered the impact of the activated gates scheme, taking into account the symmetric and asymmetric flow regimes on the discharge, and contraction coefficients, the gate leaf angle, the critical water depth, and the length of the submerged jump. The study concluded that:

- Focusing on the distinguish condition curve, the flow passed through simulated radial gates for all test runs are submerged flow.
- The discharge coefficient is uninfluenced by operated gate symmetry under constant expansion ratio.
- The derived discharge coefficient equation has good agreement with previous studies, which highlights the recorded measurements accuracy.
- The contraction coefficient increases as the gate leaf angle decreases.
- The number of operated gates is affected inversely by the gate opening, gate leaf angle, and expansion ratio.
- The length of the hydraulic jump increases with the increase in the initial Froude number. Also, the reported values are consistent with other developed formulas.
- The jump length is directly proportional to the submergence ratio.
- The gate opening has a superiority impact on the flow regime compared to the other tested variables included in the study.
- The critical water depth, the Froude No., the discharge coefficient, the length of hydraulic jump, and the submergence ratio are found to be highly sensitive to the number of activated gate openings.
- The evaluation indicator of RMSE was calculated for the comparison between developed equations and other researchers' equations for different variables, and the values were less than 10 that emphasize the high accuracy of measured data and developed equations.

It is recommended for future studies to investigate additional alternative scenarios considering the gates' functional operation under variable flow conditions to provide a thorough, comprehensive understanding of the hydraulics of radial gates.

Abbreviations

Q	Flow Discharge	[l/s]
y_t	Tailwater depth	[m]
W, G	Gate opening height	[m]
B	Flume width	[m]
b	The gate width	[m]
H_u, y_o	Upstream water depth	[m]
C_d	Discharge coefficient	[-]
b_t	Total clear width of opened gates	[m]
e	Expansion ratio	[-]
Fr_1, F_1	Froude No. at vena contacta	[-]
y_c	Critical water depth	[m]
L_j	Length of hydraulic jump	[m]
y_1, y_j	Initial water depth, minimum jet thickness (water depth at vena contracta)	[m]
y_2	Backup water depth (The instant water depth downstream the gate)	[m]
H	The head difference between upstream water depth and tailwater depth	[m]
S	Submergence ratio	[-]
g	Gravitational acceleration	[m/s^2]
θ, θ_r	Gate leaf angle	[Radian]
S_o	Bed slope	[-]
δ, δ_{sh}, Cc	Contraction coefficient	[-]
μ	Dynamic viscosity of water	[Kg/m.s]
R_e	Reynolds number	[-]
DRF	a discharge reduction factor	[-]
RMSE	Root Mean Square Error	[-]

Acknowledgements

This experiment was conducted at the Hydraulics Research Institute (HRI), National Water Research Center (NWRC), Egypt. The authors express their sincere gratitude to the institution for their collaboration throughout the experimental period. Additionally, the authors extend special appreciation to the technicians for their diligent efforts in ensuring the precise completion of the experiment.

Disclosure statement

No potential conflict of interest was reported by the author(s).

ORCID

Ahmed M. Ibraheem http://orcid.org/0000-0003-2368-7821

References

Abdel-Aal, G.M. (2004). "Modeling of rectangular submerged hydraulic jump." *Alexandria Eng. J.*, 43(6), 847–855.
Abdelhaleem, F.S.F. (2016). "Discharge estimation for submerged parallel radial gates." *Flow Meas. Instrum.*, 52, 240–245. doi:10.1016/j.flowmeasinst.2016.11.001
Abdelhaleem, F.S.F. (2017). "Hydraulics of submerged radial gates with a sill." *ISH J. Hydraul. Eng.*, 23(2), 177–186. doi:10.1080/09715010.2016.1273798

Ali, A.M., Abdelhaleem, F.S., and Elsayed, S.M. (2015). "Laboratory calibration of submerged radial gates." *8th International Engineering Conference (IEC8)*, Sharm El-Sheikh, Egypt, 17–22. https://www.researchgate.net/publication/330842379_Laboratory_Calibration_of_Submerged_Radial_Gates

Ali, A.M., ElGamal, M.H., Negm, A.M., Helwa, M.F., and Saad, M.B., 2008. "Investigating of flow characteristics downstream radial gates of naga hammadi barrages physical model." *Twelfth Int. Water Technol. Conf.* IWTC12 2008, Alexandria, Egypt.

Ali, A.M., and Mohamed, Y.A. (2010). "Effect of stilling basin shape on the hydraulic characteristics of the flow downstream radial gates." *Alexandria Eng. J.*, 49(4), 393–400. doi:10.1016/j.aej.2010.08.001

Babaei, S.S., Mohammadzadeh-Habili, J., and Zomorodian, S.M. (2021). "Experimental and theoretical modeling of a quarter-circular gate flow." *Flow Meas. Instrum.*, 80, 101983. 10.1016/j.flowmeasinst.2021.101983

Bhuiyan, F., Habibzadeh, A., Rajaratnam, N., and Zhu, D.Z. (2011). "Reattached turbulent submerged offset jets on rough beds with shallow tailwater." *J. Hydraul. Eng.*, 137(12), 1636–1648. doi:10.1061/(ASCE)HY.1943-7900.0000462

Bijankhan, M., Ferro, V., and Kouchakzadeh, S. (2013). "New stage-discharge relationships for radial gates." *J. Irrig. Drain Eng.*, 139(5), 378–387. doi:10.1061/(ASCE)IR.1943-4774.0000556

Bijankhan, M., and Kouchakzadeh, S. (2015). "The hydraulics of parallel sluice gates under low flow delivery condition." *Flow Meas. Instrum.*, 41, 140–148. doi:10.1016/j.flowmeasinst.2014.10.017

Bijankhan, M., Kouchakzadeh, S., and Bayat, E. (2011). "Distinguishing condition curve for radial gates." *J. Flow Measure Inst.*, 22(6), 500–506. doi:10.1016/j.flowmeasinst.2011.08.002

Bos, M.G. (1989). *Discharge measurement structures*. ILRI, Wageningen.

Buyalski, C.P. (1983). *Discharge algorithms for canal radial gates*. REC-ERC-83-9, Engineering and Research Center, U.S. Bureau of Reclamation, Denver, CO.

Clemmens, A.J., Strelkoff, T.S., and Replogle, J.A. (2003). "Calibration of submerged radial gates." *J. Hydraul. Eng.*, 129 (9), 680–687. doi:10.1061/(ASCE)0733-9429(2003)129:9(680)

Clemmens, A.J., and Wahl, T.L. (2012). "Computational procedures used for radial gate calibration in wingate." *World Environ. Water. Resour. Cong. ASCE* 2106–2115. doi:10.1061/9780784412312.211

Guo, X., Guo, Y., Wang, T., Fu, H., and Li, J. (2021). "Study and application of discharge calibration for submerged radial gates." *Flow Meas. Instrum.*, 78, 101912. 10.1016/j.flowmeasinst.2021.101912

Habibzadeh, A., Vatankhah, A.R., and Rajaratnam, N. (2011). "Role of energy loss on discharge characteristics of sluice gates." *J. Hydraul. Eng.*, 137(9), 1079–1084. doi:10.1061/(ASCE)HY.1943-7900.0000406

Hosny, M., Abdelhaleem, F.S., Elshenhab, A.M., and Ibrahim, A. (2025). "Prediction of discharge coefficient of submerged gates using a stacking ensemble model." *Soft Comput.* 29(3), 1911–1929. doi:10.1007/s00500-025-10518-x

Laishram, K., Devi, T.T., and Singh, N.B. 2022. "Experimental comparison of hydraulic jump characteristics and energy dissipation between sluice gate and radial gate." *Innovative trends in hydrsological environmental systems: select proceedings of ITHES 2021*, A.K. Dikshit, B. Narasimhan, B. Kumar, and A.K. Patel, eds., Springer Nature Singapore, Singapore, 207–218.

Lin, C.H., Yen, J.F., and Tsai, C.T. (2002). "Influence of sluice gate contraction coefficient on distinguishing condition." *J. Irrig. Drain Eng.*, 128(4), 249–252. doi:10.1061/(ASCE)0733-9437(2002)128:4(249)

Ma, F., Hou, Y., and Prinos, P. (2001). "Numerical calculation of submerged hydraulic jumps." *J. Hydraul. Res.*, 39(5), 493–503. 10.1080/00221686.2001.9628274

McCorquodale, J.A., and Khalifa, A.M. (1980). "Submerged radial hydraulic jump." *Hydraul. Div. ASCE*, 106(3), 355–367. doi:10.1061/JYCEAJ.0005379

Narasimhan, S., and Bhargara, P. (1976). "Pressure fluctuations in submerged jump." *J. Hydr. Div.*, 102(3), 339–350. doi:10.1061/JYCEAJ.0004490

Rahman, R.R., Karim, I.R., and Maatooq, J.S. (2020). "New approach to discharge calculation under canal radial gates." *J. Educ. Chang. Eng. Sci. Technol.*, 15(2), 792–804.

Rajaratnam, N., and Subramanya, K. (1967). "Flow equation for the sluice gate." *J. Irrig. Drain. Div.*, 93(3), 167–186. doi:10.1061/JRCEA4.0000503

Sauida, M.F. (2014). "Calibration of submerged multi-sluice gates." *Alexandria Eng. J.*, 53(3), 663–668. doi:10.1016/j.aej.2014.04.008

Sehgal, C.K. (1996). "Design guidelines for spillway gates." *J. Hydraul. Eng.*, 122(3), 155–165. doi:10.1061/(ASCE)0733-9429(1996)122:3(155)

Shayan, H.K., Farhoudi, J., and Roshan, R. (2014). "Estimation of flow discharge under the sluice and radial gates based on contraction coefficient." *Iran. J. Sci. Technol. Trans. Civ. Eng.*, 38(C2), 449–463. doi:10.22099/ijstc.2014.2421

Shayan, H.K., Farhoudi, J., and Vatankhah, A. (2021). "Experimental and field verifications of radial gates as flow measurement structures." *Water. Supply*, 21(6), 3057–3079. doi:10.2166/ws.2021.071

Swamee, P.K. (1992). "Sluice-gate discharge equations." *J. Irrig. Drain Eng.*, 118(1), 56–60. doi:10.1061/(ASCE)0733-9437(1992)118:1(56)

Tao, H., Jamei, M., Ahmadianfar, I., Khedher, K.M., Farooque, A.A., and Yaseen, Z.M. (2022). "Discharge coefficient prediction of canal radial gate using neurocomputing models: An investigation of free and submerged flow scenarios." *Eng. Appl. Comput. Fluid Mech.*, 16(1), 1–19. doi:10.1080/19942060.2021.2002721

Tel, J. 2000. "Discharge relations for radial gates." M.Sc. thesis, Delft Technical Univ, Delft.

Toch, A. (1955). "Discharge characteristics of tainter gates." *T. Am. Soc. Civ. Eng.* 120(1), 290–300. doi:10.1061/TACEAT.0007240

Yaseen, Z.M., Alawi, O.A., Alshammari, A.M., Alsuwaiyan, A., Oyedeji, M.O., and Oudah, A.Y. (2023). "Development of advanced data-intelligence models for radial gate discharge coefficient prediction: Modeling different flow scenarios." *Water. Resour. Manage.*, 37(14), 5677–5705. doi:10.1007/s11269-023-03624-8